Aerothermal Analysis of Suction Side Film Cooling in a High-Pressure Nozzle Guide Vane Cascade

AEROTHERMAL ANALYSIS OF SUCTION SIDE FILM COOLING IN A HIGH-PRESSURE NOZZLE GUIDE VANE CASCADE

M. Montis†, R. Ciorciari†, R. Niehuis†,
S. Salvadori§, M. Carnevale§, F. Martelli§

†: Institute of Jet Propulsion, University of the Federal Armed Forces Munich, Germany
§: Energy Engineering Department, University of Florence, Italy

ABSTRACT

A specific designed film-cooled nozzle guide vane cascade was tested in a high speed facility to determine the influence of suction side film cooling on the profile loss. Wake traverses with a five-hole probe and measurements of profile pressure distribution were conducted under $\mathbf{Ma_{2th}} = 0.8$ and $\mathbf{Re_{2th}} \approx 10^6$ with coolant ejection from two different rows of cooling holes located upstream of the passage throat on the suction surface. In order to clarify the differences in loss behaviour noticed between the investigated film cooling rows, numerical simulations of the experiments were carried out, allowing an in-depth comprehension of the flow phenomena taking place in the mixing layer downstream of the coolant injection point. Additional simulations of the film cooling effectiveness were conducted for both investigated rows.

NOMENCLATURE

Latin Symbols

d	hole diameter
l	vane chord
l_{ax}	vane axial chord
$\dot{m}$	mass flow rate
Ma	Mach number
p	pressure
Re	Reynolds number
s	distance along the vane profile
t	cascade pitch
T	temperature
T_{aw}	adiabatic wall temperature
T_r	recovery temperature
u	tangential coordinate
V	velocity
x	axial coordinate

Greek Symbols

ζ_{PR}	primary loss coefficient, $\zeta_{PR} = 1 - \frac{V_2^2}{V_{2,is}^2}$
ζ_{TH}	thermodynamic loss coefficient, $\zeta_{TH} = 1 - \frac{\left(1 + \frac{\dot{m}_c}{\dot{m}_m}\right) V_2^2}{V_{2,is}^2 + \frac{\dot{m}_c}{\dot{m}_m} V_{2c,is}^2}$
η_f	adiabatic film cooling effectiveness, $\eta_f = \frac{T_{aw} - T_r}{T_{tc} - T_r}$
ρ	density

Subscripts

1	inlet flow conditions (1 chord upstream of the cascade inlet)
2	downstream flow conditions (in the traversing plane)
2th	ideal downstream flow conditions (isentropic expansion to tank pressure)
c	coolant
he	hole exit
is	isentropic flow conditions
m	main flow
no	without air ejection
ref	reference conditions ($\mathrm{Ma}_{2th} = 0.8$, $\mathrm{Re}_{2th} = 1.056 \cdot 10^6$, $T_{tm} = 313.15\ K$)
sv	solid vane
t	stagnation flow conditions

Superscripts

$-$	pitch-averaged value (spanwise-averaged value for η_f)

INTRODUCTION

In order to improve energy conversion efficiency, turbine inlet temperature of gas turbines has been significantly increased in the last decades, leading to sophisticated cooling configurations for the first expansion stages. Film cooling has long established itself as standard technique to protect vane surface from the high temperature gas expanding in the first turbine stages. Since the early studies on this topic back in the 1960s, comprehensively reviewed by Goldstein (1971), a large body of literature has been published, mainly focusing on heat transfer rather than on the aerodynamic aspects of film cooling. Nevertheless, a careful design should take into account besides thermal features also aerodynamic penalty due to the interaction of the ejected air with the boundary layers of the main flow. In an attempt to estimate aerodynamic loss produced by film cooling simple models based on control volume analysis were developed, most notably by Hartsel (1972) - with subsequent modifications by Köllen and Koschel (1985), Urban et al. (1998), and Lim et al. (2010) - and by Denton (1993), who formulated the problem in terms of entropy balance. These models usually reproduce loss trend but fail to accurately predict loss, since they contain only little information about the real flow field, and should be therefore used in combination with experimental data to estimate loss variations for slight modifications of the flow conditions.

Several experimental studies addressing the effect of coolant ejection on the loss behaviour of HPT blading can be found in the technical literature: Haller and Camus (1984) measured losses due to film cooling from five separate cooling hole locations on a transonic airfoil, using carbon dioxide to simulate density ratios. According to the authors, ejection downstream of the passage throat does not generate significantly higher losses compared to prethroat ejection. Aerodynamic penalty due to film cooling from a single row in the diffusion region was also found to be insensitive to hole geometry (cylindrical or fan-shaped). Drost and Bölcs (1999) carried out measurements on a multi-row film-cooled vane and reported strong increase of loss and reduced flow turning compared to solid vane test results. They attributed this principally to thickening of the boundary layer, mainly on the SS, and to the introduction of additional pitchwise velocity components due to ejection. Jackson et al. (2000) investigated the effects of suction surface film cooling from a single row of holes using a symmetric airfoil with the same Mach number distribution on both sides. Cylindrical and conical-diffused holes were tested over a broad range of blowing and momentum flux ratios with density ratios between 0.8 and 1.3. Aerodynamic losses were found to be significantly lower with conical diffused holes, and to increase with the coolant to main flow Mach number ratio. Day et al. (1999) conducted aerodynamic loss measurements on film cooled airfoils with 14 rows of cylindrical holes at engine representative conditions. The authors reported a small efficiency reduction, which they explained with a slight thickening of the boundary layer. Further investigation replacing 8 rows of cylindrical holes with fan-shaped holes (Day et al., 1998) showed that the overall penalty associated with coolant ejection from cylindrical holes is considerably higher than with fan-shaped holes. Osnaghi et al. (1997) reported data of cascade tests carried out on a nozzle guide vane with shower head, rows of cylindrical film cooling holes on PS and SS, and trailing edge bleed. Aerodynamic loss measurements were carried out for three cooling configurations: complete cooling, coolant ejection from the shower head and trailing edge bleeding. According to the authors, coolant ejection through the shower head holes causes significant efficiency penalties even at small ejection rates . Losses due to the trailing edge bleeding were found to be almost independent from coolant mass flow rate, while the other configurations undergo a significant rise of aerodynamic penalty. In an experimental and numerical investigation that employed transonic airfoils, Urban et al. (1998) showed that losses are greatly increased by film cooling from the suction surface, whereas pressure side and trailing edge ejection produces only small changes to aerodynamic loss magnitudes. Day et al. (1999), and Osnaghi et al. (1997) indicated that density ratio influences are well correlated using the momentum flux ratio.

This study focuses primarily on the effect of suction side film cooling on loss behaviour. Ef-

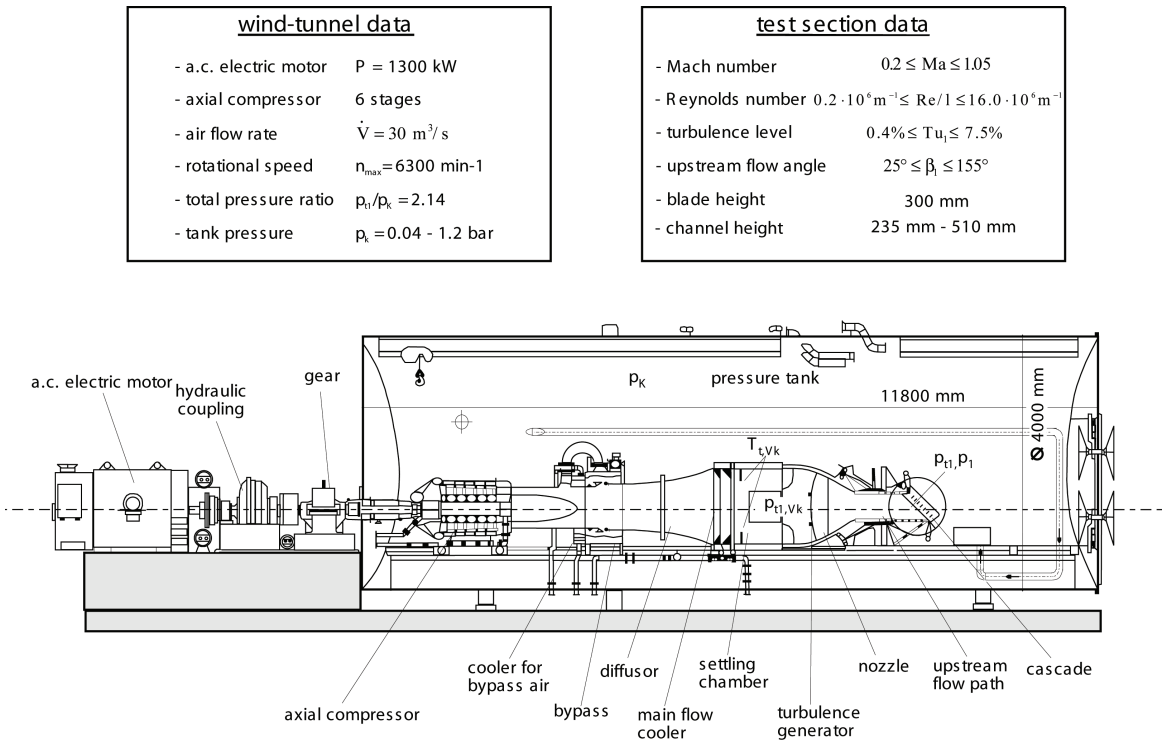

Figure 1: **Side view of the High Speed Cascade Wind Tunnel (HGK)**

fects of coolant ejection from two different rows of cooling holes are compared for several blowing ratios in terms of profile pressure distributions and total pressure losses. Experiments were backed by numerical simulations in order to obtain detailed flow field information. Additional CFD simulations, conducted in one selected case for each cooling row in order to determine the film cooling effectiveness, are reported in the last section of the paper.

EXPERIMENTAL SETUP

High Speed Cascade Wind Tunnel

Tests reported in this work were conducted at the High Speed Cascade Wind Tunnel of the Institute of Jet Propulsion of the University of the German Federal Armed Forces in Munich (fig. 1). It is a continuously operating open-loop test facility located in a cylindrical tank. This allows Mach and Reynolds numbers to be independently set by varying the tank pressure. A detailed description of the facility was given by Sturm and Fottner (1985). The turbulence grid used is known to generate under the wind tunnel settings of the present work an inlet turbulence intensity of 6%, that matches the turbulence level expected for the flow in a gas turbine. Air ejected to simulate film cooling is provided by a screw compressor. All tests with air ejection were conducted under isothermal conditions (i.e. with $T_{tc} = T_{tm}$).

Cascade Geometry

The experimental investigations were carried out on a low-solidity high-turning nozzle guide vane cascade with axial inlet flow, already subject of several studies with different objectives (Montis et al., 2009a, Montis et al., 2009b, Stephan et al., 2010). A scheme with the cascade nomenclature is shown in fig. 2. The cascade consists of five vanes with a chord length of $88.9\ mm$ and a height of $300\ mm$, whose section corresponds to the mean line profile of a typical nozzle guide vane for a heavy-duty gas turbine. Each of the three central vanes has internal plenum chambers feeding eight rows of cooling

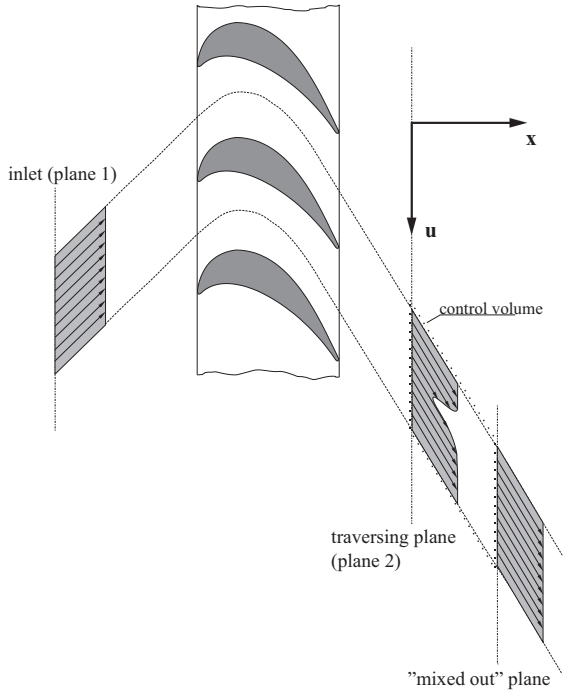

Figure 2: **Cascade scheme with nomenclature**

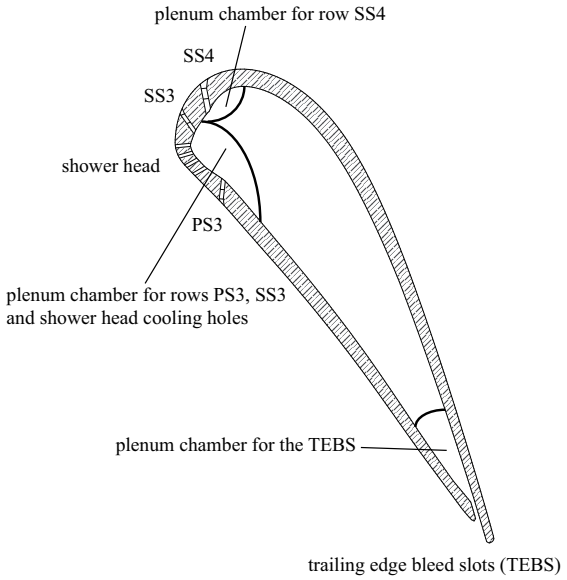

Figure 3: **Vane section (not to scale)**

holes (fig. 3): four shower head rows at the leading edge, two on the suction side (row SS3 and SS4), one on the pressure side (row PS3) and one row of trailing edge bleed slots (TEBS), discharging on the pressure side. In the present investigation, PS3 and TEBS are always closed while SS3 and SS4 are analysed separately. In order to minimise velocity in the plenum chambers, the mass flow rate of secondary air had to be limited, the cooling holes were therefore machined only over the central third of the vane height. The shower head holes are cylindrical while rows PS3, SS3 and SS4 have fan-shaped laid-back cooling holes, similar to those investigated by Gritsch et al. (1998). The inlet section diameter of the cooling holes of rows SS3 and SS4 on the suction side is $0.6\ mm$ and $0.8\ mm$ respectively, while the corresponding hole pitches are $2.68\ mm$ and $4.89\ mm$. During the tests with suction surface film cooling reported in this work, a $70\ \mu m$ thick adhesive tape was bonded to the surface of the vanes, covering row PS3 and the shower head. A solid vane was also manufactured in order to take reference measurements on the baseline geometry without cooling holes.

Instrumentation and Data Acquisition

The operating point of the wind tunnel is defined by total flow conditions upstream and static pressure downstream of the cascade. The stagnation pressure p_{t1} is measured with a Pitot probe approximately one chord length upstream of the cascade inlet section, while the stagnation temperature T_{t1} is evaluated in the settling chamber using four PT100 RTD. The reference static pressure downstream of the cascade is the tank pressure. The central vane of the cascade was instrumented with 29 pressure taps to measure the load distribution. An additional pressure tap and a PT100 RTD were positioned in each plenum of the central blade, allowing the measurement of the total conditions for the ejected air. The flow field at midspan in the wake of the central vane was measured 0.4 chord lengths downstream of the cascade exit plane using a straight five-hole pressure probe with a head diameter of $2.6\ mm$. The overall mass flow rate of air being ejected from the cooling holes was evaluated with an orifice plate mounted in the duct connecting the outlet section of the screw compressor with the plenum chambers of the cascade vanes. Model 9816 pressure transducers with 98RK scanner interface rack of Esterline Pressure Systems, Inc. were used, providing a full-scale accuracy

of $\pm 0.05\%$, while temperatures were measured with an accuracy of $\pm 0.4\ K$. The resulting relative experimental uncertainty of the flow parameters analysed in this work is $\pm 0.5\%$ for the isentropic Mach number on the vane surface (Ma_{is}), $\pm 2\%$ for the coolant mass flow rate $\dot{m}_c$, $\pm 2\%$ for the average primary loss coefficient $\overline{\zeta}_{PR}$, and $\pm 3\%$ for the average thermodynamic loss coefficient $\overline{\zeta}_{TH}$. The pitch-averaged values of the flow parameters downstream of the cascade were calculated following the standard mixed-out approach for cascade data analysis described by Amecke and Šafařik (1995), which accounts for mass, momentum, and energy conservation laws.

NUMERICAL SETUP

In order to get an insight into the flow phenomenology, the experimental analysis was backed by RANS numerical simulations conducted using the commercial code CFX-12.1 of ANSYS. Preliminary 2D simulations of the flow past the solid vane were carried out to choose the appropriate turbulence and transition models, along with a mesh sensitivity analysis. Profile loss and aerodynamic load distribution were found to be best predicted using the turbulence model SST (Menter, 1993) in combination with the transition model γ-Re_θ (Menter et al., 2006) and a structured multi-block computational grid with at least $6.5 \cdot 10^4$ cells. The SST and γ-Re_θ models were therefore employed also for the subsequent calculations with coolant ejection from rows SS3 and SS4, while the corresponding three-dimensional grid for the main flow was developed on the basis of the 2D mesh with $6.5 \cdot 10^4$ cells. The computational domain covers half of the hole pitch for both simulated configurations and the number of cells in span direction is 10 with film cooling from row SS3 and 14 with film cooling from row SS4. The final computational meshes consist of $7 \cdot 10^5$ and $9.5 \cdot 10^5$ cells respectively. Plenum chamber and cooling hole were modelled in both cases with an additional multi-block structured grid. The trailing edge slot was also modelled, knowing that the loss behaviour of an airfoil is very sensitive to changes in trailing edge geometry. The dimensionless wall distance y^+ at the wall-adjacent cell is less than 1.0 in the whole domain for all numerical simulations conducted in this study.

Boundary conditions of the cascade tests (total flow conditions and turbulence level on the inlet sections of main flow and coolant, and static pressure on the cascade outlet section) were imposed for the preliminary calculations of the flow past the solid vane and for the aerodynamic characterisation of suction side film cooling. Simulations of film cooling effectiveness were conducted under reference main flow conditions, while coolant total pressure and temperature were adjusted to match engine representative density and blowing ratios. All solid boundaries were thereby considered adiabatic.

Film cooling effectiveness simulations were additionally carried out with the in-house CFD code HybFlow, developed at the University of Florence (Adami et al., 1998, 2000).

RESULTS AND DISCUSSION

Preliminary Investigations

The results of the experimental investigations of the flow past the solid vane were used as a test case for different closure and transition models, as well as to appropriately refine the computational grid. For the sake of brevity only results obtained with the final computational settings (turbulence model SST, transition model γ-Re_θ, multi-block structured mesh with $6.5 \cdot 10^4$ cells) are reported in this section. Figure 5 shows a comparison between computed and measured load distributions at $\mathrm{Ma}_{2th} = 0.8$ for two different Reynolds numbers. The profile is front-loaded with a sharp acceleration to supersonic flow on the suction surface. The maximum isentropic Mach number on the profile is already reached at $x/l_{ax} = 0.45$. Downstream of this point the flow undergoes a long deceleration with considerable pressure recovery, which can induce boundary layer separation. Experimental results clearly indicate a longer separation bubble for the lower Reynolds number ($\mathrm{Re}_{2th} = 6.34 \cdot 10^5$), extending from $x/l_{ax} = 0.6$ to $x/l_{ax} = 0.7$. Numerical simulations are overall in good agreement

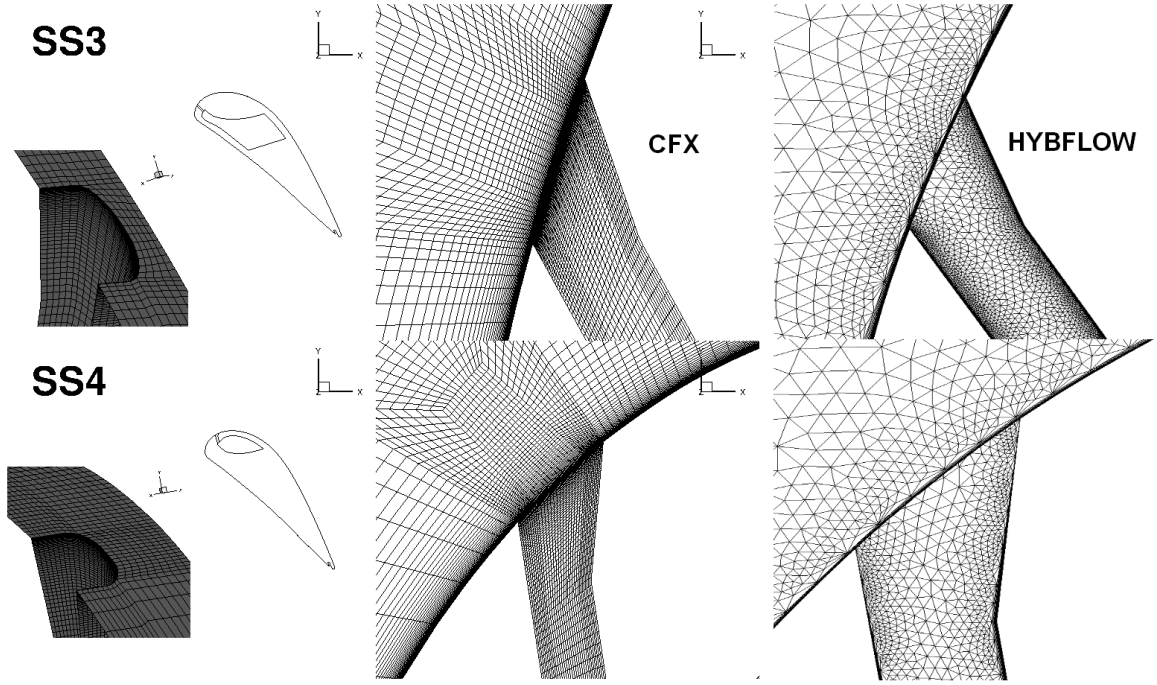

Figure 4: **Details of the computational grid in the cooling zones**

with the experiments. At $\mathrm{Re}_{2th} = 6.34 \cdot 10^5$ a larger extent of the separated flow region than at $\mathrm{Re}_{2th} = 1.056 \cdot 10^5$ is correctly predicted, even though compared to the experimental data the reattachment point is shifted 10% of the axial chord downstream, which seems to be the cause of the slight underestimation of the isentropic Mach number on the profile between the sonic line ($x/l_{ax} = 0.25$) and the separation point. Figure 6 compares predicted and measured average loss $\overline{\zeta}_{PR}$ of the flow past the solid vane under different Reynolds and Mach numbers. Data are normalised to the experimental pitch-averaged primary loss under reference conditions. Both the rise of profile loss at lower Reynolds number and the decreasing trend of $\overline{\zeta}_{PR}$ with increasing outlet Mach number are quite well reproduced by the numerical simulations, the former being generated by the longer separation bubble at lower Re_{2th}, while the latter is a typical trend for front-loaded high pressure turbine airfoils in transonic regime. A likely explanation for such loss behaviour is that as Ma_{2th} is increased, the extent of the region with adverse pressure gradient at the rear of the airfoil is reduced, producing thinner boundary layers, while as long as the outlet Mach number remains subsonic, almost no additional loss is generated through the shock deceleration. Similar results were obtained from Corriveau et al. (1998), Jouini et al. (2002) and Wolf et al. (2010). In tests conducted on different high pressure front-loaded turbine cascades with outlet Mach numbers ranging from 0.5 to 1.3 they all found a minimum of total pressure loss for Mach number approaching 1.0.

Vane Aerodynamics with Suction Side Coolant Ejection

The effect of suction side film cooling on the loss behaviour of the cascade was investigated considering four different blowing conditions for each cooling row, with a ratio p_{tc}/p_{he} of the total pressure in plenum to the static pressure at the hole exit section ranging from 1.1 to 1.7, as reported in tables 1 and 2. All measurements and computation were carried out under main flow reference conditions. Figure 7 shows load distribution and primary loss in the wake of the airfoil with coolant ejection from row SS3 at $p_{tc}/p_{he} = 1.11$ (figs. 7a and 7b) and from row SS4 at $p_{tc}/p_{he} = 1.32$ (figs. 7c and 7d). In both cases the momentum ratio $(\rho_c V_c^2)/(\rho_m V_m^2)$, which is generally considered the scaling

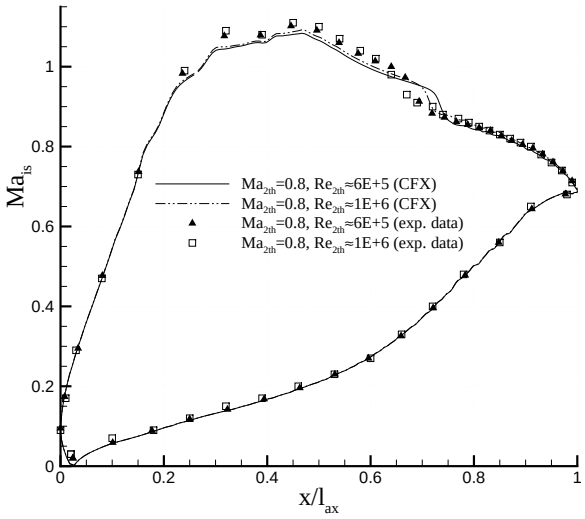

Figure 5: **Effect of Reynolds number on the isentropic Mach number distribution of the solid vane**

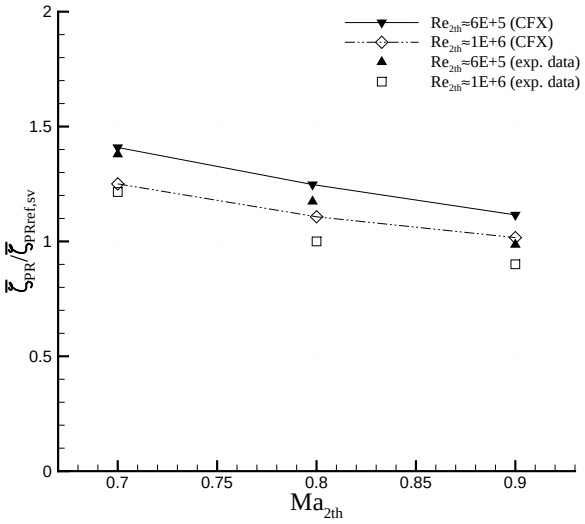

Figure 6: **Mean value of primary loss coefficient as a function of outlet Mach number for different Reynolds numbers**

$\frac{p_{tc}}{p_{he}}$	$\frac{\dot{m}_c}{\dot{m}_2}$	$\frac{\rho_c V_c}{\rho_m V_m}$	$\frac{\rho_c V_c^2}{\rho_m V_m^2}$
1.11	0.204%	1.68	2.75
1.31	0.344%	2.86	7.57
1.51	0.431%	3.65	11.9
1.71	0.503%	4.29	15.8

Table 1: **Local blow parameters for the tests with air ejection from row SS3**

$\frac{p_{tc}}{p_{he}}$	$\frac{\dot{m}_c}{\dot{m}_2}$	$\frac{\rho_c V_c}{\rho_m V_m}$	$\frac{\rho_c V_c^2}{\rho_m V_m^2}$
1.12	0.161%	0.80	0.64
1.32	0.295%	1.31	1.65
1.53	0.373%	1.67	2.56
1.73	0.436%	1.95	3.38

Table 2: **Local blow parameters for the tests with air ejection from row SS4**

parameter for aerodynamic loss, is representative of engine conditions. The computed isentropic Mach number distributions on the vane surface completely match the experimental results. Even in the region with adverse pressure gradient on the suction side as well as in the supersonic region very good agreement between numerical simulation data and experiments is achieved. The coolant ejection trips the boundary layer on the SS, so that, unlike for the solid vane, the boundary layer is already turbulent before the maximum of Ma_{is} and has therefore enough momentum to overcome the adverse pressure gradient, remaining attached over the entire suction surface. The influence of film cooling on the pressure distribution on the profile, although more evident for row SS4, is in both cases confined to the cooling row near-region, with a slight blockage effect on the oncoming flow and a noticeable acceleration downstream of the cooling holes, due to the local increase of the streamline curvature of the mainflow produced by the cooling jets.

As shown in figs. 7b and 7d the loss distribution downstream of the cascade is quite well predicted both with film cooling from row SS3 and from row SS4. Measured and computed loss are normalised to the mixed-out primary loss coefficient $\overline{\zeta}_{PRref,no}$ obtained in the experiments without coolant ejection under reference conditions. This turned out to be 43% higher than for the solid vane, primarily due to the modified trailing edge geometry, as reported in a previous study (Montis et al., 2009). In both cases the maximum of ζ_{PR} obtained from the simulations matches very closely the experimental data, while the wake width is slightly underestimated. The likely cause for such discrepancy is the

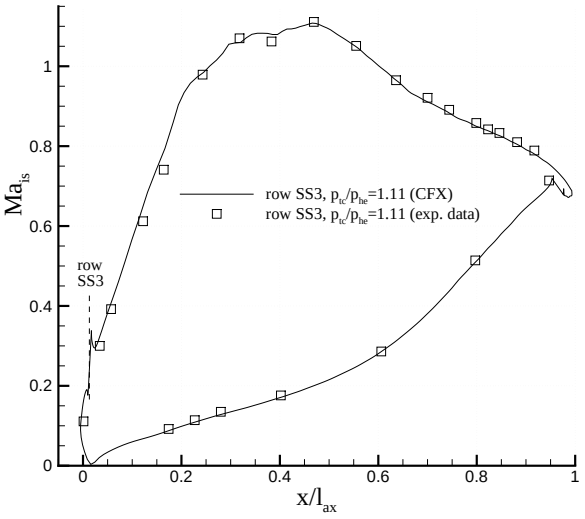

(a) **Row SS3, $\mathbf{p_{tc}/p_{he} = 1.11}$**

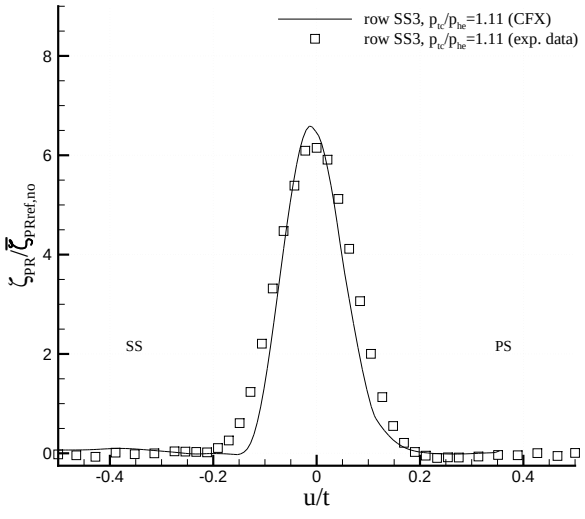

(b) **Row SS3, $\mathbf{p_{tc}/p_{he} = 1.11}$**

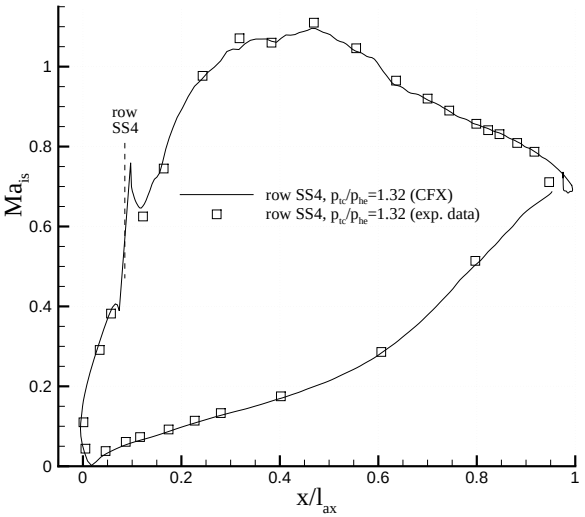

(c) **Row SS4, $\mathbf{p_{tc}/p_{he} = 1.32}$**

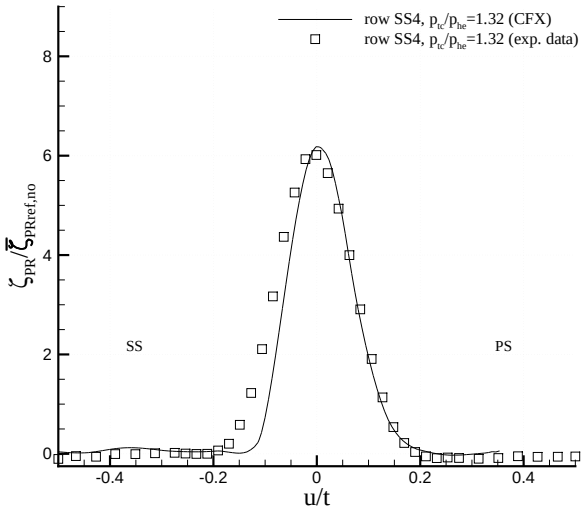

(d) **Row SS4, $\mathbf{p_{tc}/p_{he} = 1.32}$**

Figure 7: **Measured and predicted aerodynamic loading of the profile and loss distribution downstream of the cascade with coolant ejection from row SS3 (figs. 7a and 7b) and from row SS4 (figs. 7c and 7d) under $\mathbf{Ma_{2th} = 0.8}$, $\mathbf{Re_{2th} = 1.056 \cdot 10^6}$, $\mathbf{T_{tc} = T_{tm} = 313.15\ K}$**

adhesive tape bonded to the vane surface. This could trip the boundary layer on the pressure side, which would normally remain laminar until the trailing edge, causing additional loss.

Figure 8 shows the mixed-out profile loss with film cooling from row SS3 (fig. 8a) and SS4 (fig. 8b) for all blowing conditions investigated. Beside the primary loss coefficient also the thermodynamic loss coefficient is presented here, a common loss parameter accounting for the kinetic energy contribution of coolant ejection. As pointed out by many authors (Mee, 1992 and Osnaghi et al., 1997, among others), the momentum contribution of the ejected coolant should always be considered in order to assess the performance of a cooled airfoil, since the primary loss coefficient is in that case merely a measure of the kinetic energy in the wake. Data are again normalised to the experimental loss without film cooling $\overline{\zeta}_{PRref,no}$. In both cases the trends of $\overline{\zeta}_{PR}$ and $\overline{\zeta}_{TH}$ as a function

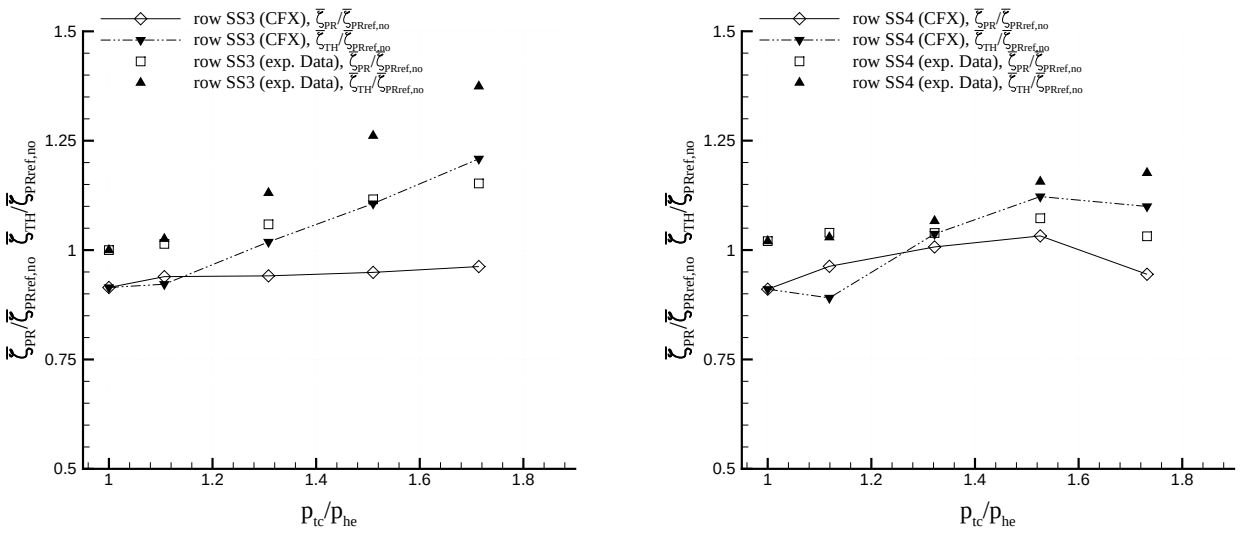

Figure 8: **Average primary and thermodynamic loss as a function of $\mathbf{p_{tc}/p_{he}}$ with coolant ejection from row SS3 (fig. 8a) and from row SS4 (fig. 8b) under $\mathbf{Ma_{2th} = 0.8}$, $\mathbf{Re_{2th} = 1.056 \cdot 10^6}$, $\mathbf{T_{tc} = T_{tm} = 313.15\ K}$**

of the pressure ratio across cooling holes p_{tc}/p_{he} are well reproduced, with a slight underestimation already noticed in the local loss distributions of fig. 7. The two investigated film cooling rows show a different influence on the loss behaviour of the airfoil. Coolant ejection from row SS3 produces an increase with almost constant gradient of $\overline{\zeta}_{PR}$ and $\overline{\zeta}_{TH}$ as the pressure ratio across the cooling holes is raised from $p_{tc}/p_{he} = 1.1$ to $p_{tc}/p_{he} = 1.7$, while the loss characteristics with film cooling from row SS4 exhibit a maximum at $p_{tc}/p_{he} = 1.5$. An analysis of the velocity streamline plots presented in fig. 9 can help to explain such differences. Two plots are shown exemplarily for each cooling row, representative of low and high blowing ratio conditions. Comparing fig. 9a and fig. 9b it can be observed that the flow pattern for the coolant ejection remains qualitatively unchanged. The flow in the hole duct remains attached at low as well as at high p_{tc}/p_{he}, and the only effect of the higher blowing ratio is to extend the recirculation zone downstream of the injection point and to strengthen the jet lift-off, which actually already takes place at low blowing ratio. At row SS4, unlike at row SS3, coolant is injected in a strong crossflow that produces an effective blockage of the film cooling jets at low blowing ratio (fig. 9c). Considerable pressure recovery takes place in the hole duct and the flow separates at the edge of the laid-back hole expansion, however, the recirculation zone is almost completely confined to the hole duct. As the total pressure in the plenum chamber is increased (fig. 9d) the jet is lifted off and the separated flow region moves outside of the duct to the vane surface, which explains the noticeable growth of profile loss between $p_{tc}/p_{he} = 1.1$ and $p_{tc}/p_{he} = 1.5$. For higher pressure ratios the flow pattern doesn't change significantly and the large momentum contribution of the film cooling jets exceeds the additional loss, leading to a net reduction of $\overline{\zeta}_{PR}$. Despite the complex flow patterns shown in fig. 9 the coolant mass flow rate (i.e. the discharge coefficient of the cooling holes) correctly predicted for both rows at all blowing ratios (fig. 10).

Heat Transfer Analysis

The last part of the study was focused on the numerical simulation of the heat transfer on the vane surface. Two RANS calculations of the film cooling effectiveness were conducted under reference main flow conditions ($\mathrm{Ma}_{2th} = 0.8$, $\mathrm{Re}_{2th} = 1.056 \cdot 10^6$, $T_{tm} = 313.15\ K$), adjusting coolant total

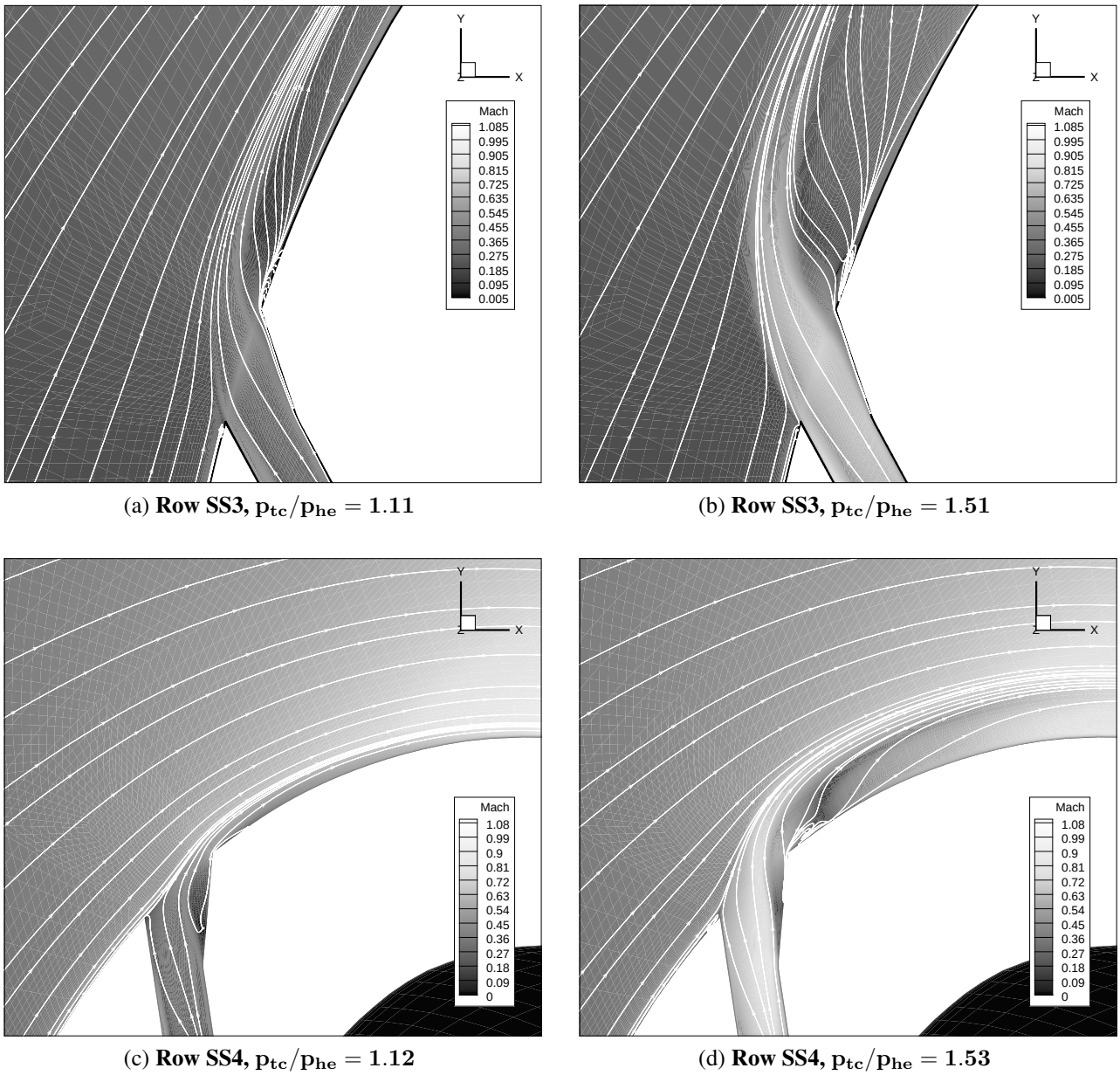

(a) **Row SS3, $\mathbf{p_{tc}/p_{he} = 1.11}$**

(b) **Row SS3, $\mathbf{p_{tc}/p_{he} = 1.51}$**

(c) **Row SS4, $\mathbf{p_{tc}/p_{he} = 1.12}$**

(d) **Row SS4, $\mathbf{p_{tc}/p_{he} = 1.53}$**

Figure 9: **Velocity streamlines in the coolant ejection region for rows SS3 and SS4 under main flow reference conditions ($\mathbf{Ma_{2th} = 0.8}$, $\mathbf{Re_{2th} = 1.056 \cdot 10^6}$, $\mathbf{T_{tc} = T_{tm} = 313.15\ K}$) and different blowing conditions**

pressure and temperature of each cooling row in order to obtain engine representative density and blowing ratios (see tab. 3). Since no heat transfer experimental data are available for the investigated airfoil, the academic code HybFlow of the University of Florence was used as a benchmark. Results are presented in fig. 11 in terms of film cooling effectiveness maps on the vane surface and spanwise-averaged values along the profile.

Film cooling from row SS3 and row SS4 show fairly different characteristics. Coolant ejected from the former row exhibits almost no tendency to diffuse and merge with the neighbour jets (fig. 11a), while film cooling from the latter produces - despite the unfavourable pitch to diameter ratio - a noticeable better coverage in the far downstream region (fig. 11b). In the near-hole region of row SS4 are observed lower values of film cooling effectiveness than expected, suggesting that the mainflow

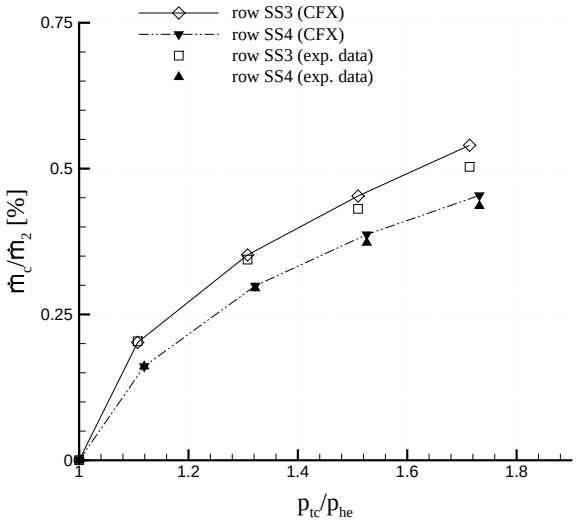

Figure 10: **Coolant mass flow rate as a function of $\mathbf{p_{tc}/p_{he}}$ for rows SS3 and SS4 ($\mathbf{Ma_{2th} = 0.8}$, $\mathbf{Re_{2th} = 1.056 \cdot 10^6}$, $\mathbf{T_{tc} = T_{tm} = 313.15\ K}$)**

	Row SS3	Row SS4
Re_{2th}	$1.056 \cdot 10^6$	$1.056 \cdot 10^6$
Ma_{2th}	0.80	0.80
T_{tm}	313.15 K	313.15 K
T_{tc}	130.0 K	137.8 K
p_{tc}/p_{he}	1.05	1.24
ρ_c/ρ_m	2.4	2.3
$(\rho_c V_c)\ /\ (\rho_m V_m)$	1.8	1.7
$(\rho_c V_c^2)\ /\ (\rho_m V_m^2)$	1.35	1.26

Table 3: **Simulated flow conditions for the numerical investigation of film cooling effectiveness**

could entrain the injection zone immediately downstream of the cooling hole.

The spanwise-averaged values of film cooling effectiveness $\overline{\eta}_f$ are consistent with the maps of fig. 11a and 11b. For row SS3 $\overline{\eta}_f$ is monotonically decreasing (fig. 11c), while for row SS4 it shows a local minimum at approximately $s/d = 2$ and higher values far downstream (fig. 11d). The results of the simulation with HybFlow exhibit qualitatively the same trends obtained with CFX, although with overall lower values of $\overline{\eta}_f$.

CONCLUSIONS

Extensive experimental and numerical investigations were carried out on a film-cooled nozzle guide vane cascade to determine the influence of suction side film cooling on the profile loss. RANS simulations proved to be a valid tool to accurately predict loss produced by coolant ejection under different blowing conditions, and also provided reliable flow field data, allowing a correct interpretation of the physical phenomena taking place in the mixing layer downstream of the coolant injection point. Numerical simulation were finally extended to the heat transfer problem, gathering significant information on the film cooling performance of the investigated rows of cooling holes.

ACKNOWLEDGEMENTS

The experiments were conducted as a part of the joint research programme COOREFF-T in the frame of AG Turbo. The work was supported by the Bundesministerium für Wirtschaft und Technologie (BMWi) as per resolution of the German Federal Parliament under grant number 0327713D. The authors gratefully acknowledge AG Turbo and Alstom for their support and permission to publish this paper. The responsibility for the content lies solely with its authors.

REFERENCES

Adami, P., Michelassi, V. and Martelli, F. (1998), *"Performances of a Newton-Krylov scheme against implicit and multigrid solvers for inviscid flows"*, AIAA paper 98-2429

Adami, P., Martelli, F. and Michelassi, V. (2000), *"Three-Dimensional Investigations for Axial*

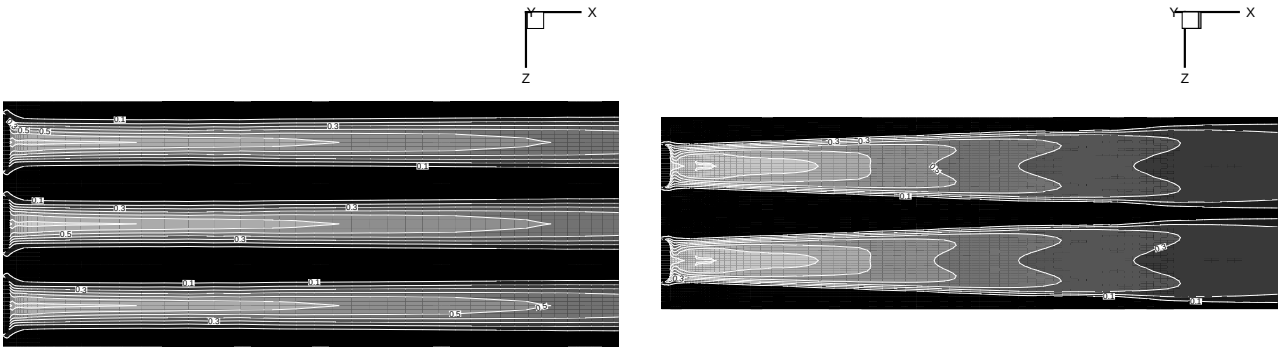

(a) **Film cooling effectiveness map (SS3)**

(b) **Film cooling effectiveness map (SS4)**

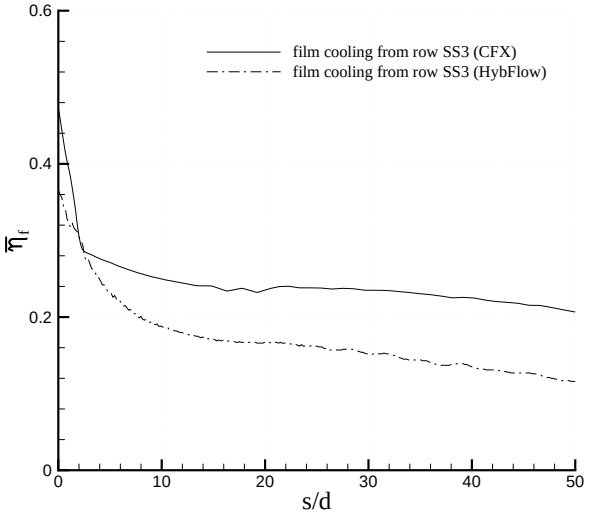

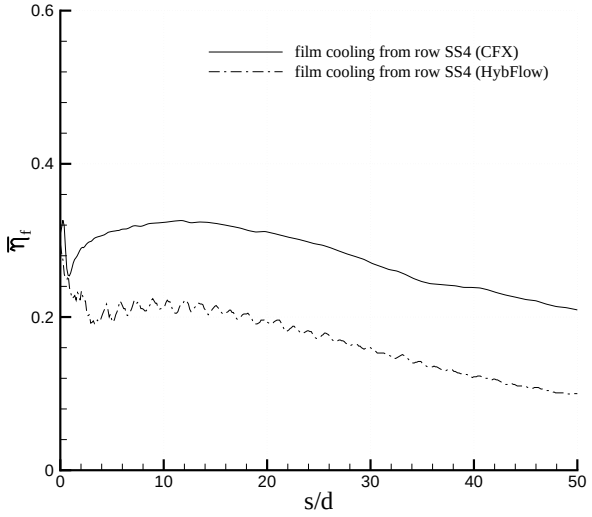

(c) **Spanwise-averaged film cooling effectiveness (SS3)**

(d) **Spanwise-averaged film cooling effectiveness (SS4)**

Figure 11: **Film cooling effectiveness downstream of the rows of cooling holes SS3 and SS4 under the flow conditions listed in tab. 3**

Turbines by an Implicit Unstructured Multi-Block Flow Solver", ASME paper 2000-GT-0636

Amecke, J. and Šafařík, P. (1995), *"Data reduction of wake flow measurements with injection of another gas"*, Report 95-32, Deutsche Forschungsanstalt für Luft- and Raumfahrt, Cologne

Corriveau, D. and Sjolander, S. A. (2004), *"Influence of Loading Distribution on the Performance of Transonic High Pressure Turbine Blades"*, ASME J. Turb., vol. 126 pp. 288-296

Day, C. R. B., Oldfield, M. L. G. and Lock, G. D. (1999), *"The Influence of Film Cooling on the Efficiency of an Annular Nozzle Guide Vane Cascade"*, ASME J. Turb., vol. 121 pp. 145-151

Day, C. R. B., Oldfield, M. L. G., Lock, G. D. and Dancer, S. N. (1998), *"Efficiency Measurements of an Annular Nozzle Guide Vane Cascade with Different Film Cooling Geometries"*, ASME paper 98-GT-538

Denton, J. D. (1993), *"Loss Mechanisms in Turbomachines"*, ASME J. Turb. vol. 115 pp.

621-656

Drost, U. and Bölcs, A. (1999), *"Performance of a Turbine Airfoil with Multiple Film Cooling Stations, Part II: Aerodynamic Losses"*, ASME paper 99-GT-42

Goldstein, R. J. (1971) *"Film Cooling"*, Advances in Heat Transfer, vol. 7 pp. 321-379

Gritsch, M., Schulz, A. and Wittig, S. (1998), *"Discharge Coefficient Measurements of Film-Cooling Holes With Expanded Exits"*, ASME J. Turb., vol. 120 pp. 557-563

Haller, B. R. and Camus, J. J. (1984), *"Aerodynamic Loss Penalty Produced by Film Cooling in Transonic Turbine Blades"*, ASME J. Eng. Gas Turbines Power, vol. 106 pp. 198-205

Hartsel, J. E. (1972), *"Prediction of Effects of Mass-Transfer Cooling on the Blade-Row Efficiency of Turbine Airfoils"*, AIAA paper 72-11

Jackson, D. J., Lee, K. L., Ligrani, P. M. and Johnson, P. D. (2000), *"Transonic Aerodynamic Losses Due to Turbine Airfoil, Suction Surface Film Cooling"*, ASME J. Turb. vol. 122 pp. 317-326

Jouini, D. B. M., Sjolander, S. A. and Moustapha, S. H. (2002), *"Midspan Flow-Field Measurements for Two Transonic Linear Turbine Cascades at Off-Design Conditions"*, ASME J. Turb. vol. 124 pp. 176-186

Köllen, O. and Koschel, W. (1985), *"Effect of Film Cooling on the Aerodynamic Performance of a Turbine Cascade"*, AGARD CP-390, paper 39

Lim, C. H., Pullan, G. and Northall, J. (2010), *"Estimating the Loss Associated with Film-Cooling for a Turbine Stage"*, ASME paper GT2010-22327

Mee, D. J. (1992), *"Techniques for Aerodynamic Loss Measurement of Transonic Turbine Cascades With Trailing-Edge Region Coolant Injection"*, ASME paper 92-GT-157

Menter, F. R. (1993), *"Zonal two equation k-ω turbulence models for aerodynamic flows"*, AIAA paper 93-2906

Menter, F. R., Langtry, R. B., Likki, S. R., Suzen, Y. B., Huang, P. G. and Völker, S. (2006), *"A Correlation-Based Transition Model Using Local Variables - Part I: Model Formulation"*, ASME J. Turb. vol. 128 pp. 413-422

Montis, M., Niehuis, R. and Stephan, B. (2009a), *"Experimental Investigation of the Influence of Cooling Air Injection on the Aerodynamics of a High Pressure NGV-Cascade"*, paper presented at the VIII European Turbomachinery Conference, Graz, Austria

Montis, M., Niehuis, R., Guidi, M., Salvadori, S., Martelli, F. and Stephan, B. (2009b), *"Experimental and Numerical Investigation of the Influence of Trailing Edge Bleeding on the Aerodynamics of a NGV Cascade"*, ASME paper GT2009-59910

Osnaghi, C., Perdichizzi, A., Savini, M., Harasgama P. and Lutum, E. (1997), *"The Influence of Film-Cooling on the Aerodynamic of a Turbine Nozzle Guide Vane"*, ASME paper 97-GT-522

Stephan, B., Krückels, J., and Gritsch, M. (2010), *"Investigation of Aerodynamic Losses and Film Cooling Effectiveness for a NGV Profile"*, ASME paper GT2010-22810

Sturm, W. and Fottner, L. (1985), *"The High-Speed Cascade Wind Tunnel of the German Armed Forces University Munich"*, paper presented at the VIII Symposium on Measuring Techniques for Transonic and Supersonic Flows in Cascades and Turbomachines, Genoa, Italy

Urban, M. F., Hermeler, J. and Hosenfeld, H. G. (1998), *"Experimental and Numerical Investigations of Film-Cooling Effects on the Aerodynamic Performance of Transonic Turbine Blades"*, ASME paper 98-GT-546

Wolf, T., Kost, F., Janke, E., Haselbach, F. and Willer, L. (2010), *"Experimental and Numerical Studies on Highly Loaded Supersonic Axial Turbines Cascades"*, ASME paper GT2010-23808